

# Spatial and seasonal differences between near surface air temperature and land surface temperature for Urban Heat Island effect assessment



Yanfen Xiang<sup>a</sup>, Bohong Zheng<sup>a</sup>, Komi Bernard Bedra<sup>a</sup>, Qianli Ouyang<sup>a</sup>, Junyou Liu<sup>a</sup>, Jian Zheng<sup>b,\*</sup>

<sup>a</sup> School of Architecture and Art, Central South University, Changsha 410083, China

<sup>b</sup> School of Architecture, Changsha University of Science and Technology, Changsha 410114, China

## ARTICLE INFO

### Keywords:

Surface air temperature  
Land surface temperature  
Landsat 8–9  
Urban Heat Island intensity  
Correlation analysis

## ABSTRACT

In the context of global warming, urban thermal environments are a growing concern. Previous studies focused on Urban heat island effect and global warming mitigation amplitude with Land Surface Temperature (LST), ignoring the interaction of LST and Surface Air Temperature (SAT), which comprehensively affects pedestrian thermal comfort. This study examines the SAT-LST relationship to reduce the uncertainty about SAT prediction based on LST. Utilizing data from 280 air temperature sensors and Landsat satellite remote sensing, we quantified temporal and spatial variations between SAT and LST in Changsha (under a monsoon climate). Analyzing data from 2018 to 2022, the study found that: 1) There are spatiotemporal differences in the SAT-LST relationship, with strong spatial heterogeneity, notably in urban areas and during the summer; 2) A stronger correlation between SAT and LST in winter ( $R^2 = 0.916$ , RMSE = 1.242 °C) than in summer ( $R^2 = 0.500$ , RMSE = 1.517 °C); 3) UHI and SUHI also exhibit spatiotemporal variations, with the cold and hot spots in summer not completely overlapping spatially. By constructing an SAT-LST regression model, the study deepens the understanding of the quantitative relationships between SAT and LST, thus contributing to urban thermal environment research and climate adaptive urban planning and design.

## 1. Introduction

Climate change has become a central focus of the global community, especially in the context of urbanization. As cities transition from natural to manufactured environments, they bring forth the threats of heatwaves and urban heat islands. Undoubtedly, human activities contribute to climate change (Intergovernmental Panel On Climate (IPCC), 2021), and the synergistic effects of heatwaves and urban heat islands exacerbate the deterioration of urban thermal environments (He et al., 2022). Over the past two decades, the number of deaths from heat wave-related diseases in China has quadrupled (Liu et al., 2021). Frequent extreme weather events have emerged as a significant threat in the context of global warming.

\* Corresponding author at: School of Architecture, Changsha University of Science and Technology, 45 Chiling Road, Changsha City, Hunan Province, China.

E-mail address: [1693880934@qq.com](mailto:1693880934@qq.com) (J. Zheng).

China's annual average temperature has been increasing at a rate of 0.26 °C per decade, far exceeding the global average of 0.15 °C per decade during the same period (Intergovernmental Panel On Climate (IPCC), 2021). This makes China a sensitive region to global climate change. Hence, optimizing China's urban heat island effect has become an urgency.

Cities play a pivotal role in facilitating thermal mitigation strategies and human adaptation measures. The transformation of urban land use patterns and morphological characteristics has significantly increased urban temperatures, resulting in higher temperatures in urban than in suburb, thereby forming the Urban Heat Island (UHI) (Manley, 1958). The UHI directly or indirectly affects the thermal comfort and well-being of urban inhabitants (Basu and Ostro, 2008; Oke, 1982). Consequently, an increasing number of scholars are focusing on UHI, utilizing it to assess and improve the urban thermal environment (Manoli et al., 2019; Oke et al., 1991). The quantification of UHI in most studies relies on two primary temperature metrics: (a) the Surface Air Temperature (SAT) and (b) the Land Surface Temperature (LST) (Mirzaei, 2015). (a) SAT refers to the temperature at pedestrian height within the urban canopy, typically measured by fixed ground-based meteorological stations or mobile measurements (Coseo and Larsen, 2014; Ivajnsic et al., 2014). Urban Heat Island Intensity (UHII) is calculated as the spatially-averaged surface air-temperature difference between urban and suburb areas (Memon et al., 2009). (b) LST originate from airborne or satellite-borne sensors (Hu and Brunsell, 2015; Reiners et al., 2023). These sensors measure the temperature of the land surface as seen from above, and this temperature is related to the air temperature in the same location. The Surface Urban Heat Island Intensity (SUHII) quantifies the LST discrepancy between urban and suburb areas (Voogt and Oke, 2003).

Both SAT and LST have limitations when used for studying the urban heat island effect. SAT not only serves as an important parameter for describing the thermal environment of urban, but also reflects the thermal perception of urban residents (Sheng et al., 2017; Van Tol and Ellis, 2023). These data are often obtained through ground-based observations, allowing scholars to compare the thermal environments (Kousis et al., 2023) and thermal comfort (Huang et al., 2023; Xu et al., 2023) across different urban spaces. Since the British meteorologist Howard (1833) recorded temperature variations in the city of London in 1811, researchers have relied on temperature data for over a century. It was in 1972 when Rao pioneered the application of remote sensing in studying Urban Heat Island effects. The utilization of remote sensing has greatly expanded the scope of research, enabling researchers to transition from localized to global studies (Chen et al., 2023b; Reiners et al., 2023). Throughout these investigations, it has become evident that both SAT and LST possess distinct advantages and limitations. SAT data boasts extended periods of observation, permitting time-series studies, and closely aligns with temperatures perceived by humans, rendering it valuable for spatial suitability design. However, it is constrained by factors such as limited distribution of urban weather stations, low spatial resolution, scale effects, high budget and manpower requirements for data collection, and challenges in explaining and characterizing the complex spatial distribution within cities. Consequently, contemporary researchers (Schwarz et al., 2012; Sheng et al., 2017; Sun et al., 2020; Yang et al., 2019) rely on limited meteorological station data for urban thermal environment studies. LST data offer the advantages of expansive coverage and high spatial resolution, but remains susceptible to cloud cover or atmospheric interference. Moreover, high spatial resolution LST data often comes sacrifices temporal resolution, and vice versa.

To address these limitations, researchers have proposed several methods. Firstly, they have employed Spatial Interpolation Methods. For instance, Eldrandaly and Abu-Zaid (2011) and Di Piazza et al. (2015) have utilized interpolation methods like Regression Kriging (RK), PRISM, Anusplin, and other methods to improve the interpolation accuracy (Daly et al., 1997; Jeffrey et al., 2001). It's important to note that this approach is better suited for research at provincial scales and beyond, and it is higher levels of uncertainty in urban built-up areas (Good, 2015). The second method involves integrating mobile measurements and fixed meteorological stations' measurements to achieve higher spatial resolution (Goldblatt et al., 2021; Nichol and Wong, 2008). However, this approach suffers from limited concurrency, demanding and labor-intensive long-term data collection, substantial budget requirements, and the involvement of significant human and material resources. The third approach involves Statistical Methods, specifically build an estimation model. Common techniques include Simple Statistical Models, Multiple Linear Regression Models, and Machine Learning Methods. Machine Learning can handle non-linear and highly correlated predictors variables and estimate the temperature in areas, mainly including Neural networks, Random forests, CNN, and ANN have been employed to explore the relationship between predictor variables and temperature (Chen et al., 2023a; Liu et al., 2021a). This method is particularly suitable for constructing predictive models with multiple factors, but it has limitations due to its internal "black-box" model, which conceals the underlying mechanisms. Studies have shown that the Linear regression models are more accurate in calculating the average daily temperature with a Root Mean Square Error ranging between 1.29 and 3.60 °C (Shi et al., 2016; Yang et al., 2017b).

There is a correlation between LST and SAT, but the impact of the urban heat island effect within cities is inconsistent. Vogt et al. (1997) propose that accurate mapping of SAT distribution is possible. It is commonly assumed that the variability in the land surface response forces the atmosphere significantly, influencing the SAT variability due to changes in LST. The scholars carried out research in cities at different latitudes, including Bucharest, Romania (Cheval and Dumitrescu, 2015), Los Angeles (Shiflett et al., 2017), Leipzig, Germany (Schwarz et al., 2012), Shenzhen, China (Cao et al., 2021) and other cities. They used remote sensing data such as Aqua, AVIRIS, MODIS/ASTER, Landsat, and SAT data for correlation analysis, and the study results confirmed a strong correlation between LST and SAT. However, they also found variations in LST and SAT, particularly in different regions, seasons, and regarding the Urban Heat Island effect. The primary influencing factor was the spatial heterogeneity of urban areas. Therefore, it is necessary to explore the variations in LST and SAT within different spatial contexts.

Current research on the urban heat island effect often relies on limited SAT data, with study durations ranging from several days to several years (Sheng et al., 2017; Stisen et al., 2007; Vogt et al., 1997). Is the scarcity of data causing spatial and temporal changes in the UHI to be inconsistent with the SUHI? Do seasonal variations persist when there is a sufficient amount of meteorological station data? Addressing these questions is crucial because temperature is a key variable influencing human thermal comfort and health (He et al., 2021). This not only enhances our understanding of the spatial heterogeneity of urban thermal environments but also provides

support for urban planning and natural resource management aimed at mitigating extreme heat caused by Urban Heat Islands and adapting to climate change.

In this study, we have selected Changsha, a city known for its typical cold winters and hot summers, as our research subject. By analyzing data from the past four years, we aim to explore the spatial and seasonal variations of UHI and SUHI. This research contributes to the development of strategies for mitigating urban heat effects and designing urban climate adaptation plans.

## 2. Date and methods

### 2.1. Study area

Considering that the influencing factors involve seasonal differences, a city with significant differences in winter and summer is selected as the research object. Affected by the unique geographical environment and the East Asian monsoon, compared with other countries at the same latitude, the average temperature in China is 10 °C lower in winter, and the average temperature in summer is 3 °C higher. Therefore, Changsha City, with typical cold winter and hot summer characteristics, was selected as the research object.

Changsha is the capital city of Hunan Province, China (Fig. 1), with a latitude of 27.51' - 28.40' north, a longitude of 111.54' - 114.15' east, and an altitude of 23.5 m to 1607.9 m. The central part of the city has the Xiangjiang River running through it from south to north, so the terrain is low in the middle and high in the east and west. In 2020, the city's land area was 11,816.0 km<sup>2</sup>, governing 6 districts, 1 county, and hosting 2 county-level cities. The research scope covers the entire urban area of Changsha. The research area includes built-up areas and suburb, a city with significant spatial variation characteristics. This region is located in the northern subtropical zone and is significantly affected by the monsoon circulation. It is dominated by low-latitude oceanic warm and humid air masses in summer, with high humidity and hot summer weather. The extremely high temperature has reached 43.0 °C over the years. Winter is controlled by Siberia's cold and humid air mass, causing rain, snow, and frost, and the historically extremely low temperature reaches -5.0 °C.

## 2.2. Data

### 2.2.1. Surface air temperature

Determine the months of summer and winter in Changsha. Many researchers have been trying to study the temperature change index in recent decades and found that global warming does not increase exponentially, and the relationship between SAT and LST should be analyzed from the data of recent years (Xiong and Chen, 2017), so the past seventeen years' data were selected for analysis. The air temperature data, downloaded from Changsha Meteorological Bureau (<http://hn.cma.gov.cn/dsqx/zss/>), were chosen from 2006 to 2022 (Fig. 2) to analyze the city's monthly temperature changes. The annual average temperature in Changsha City is 18.02 °C, and the average temperature in June, July, and August in summer is relatively high. The highest average temperature in July is 29.60 °C, and the extreme temperature is as high as 43 °C. In winter, the temperature in January, February, and December is relatively low. The lowest average temperature in January is 5.21 °C, and the extreme temperature is as low as -5 °C. It can be seen that Changsha city is a typical city with hot summer and cold winter, so the data collection of this study should be concentrated on January to February and December in winter, and June to August in summer.

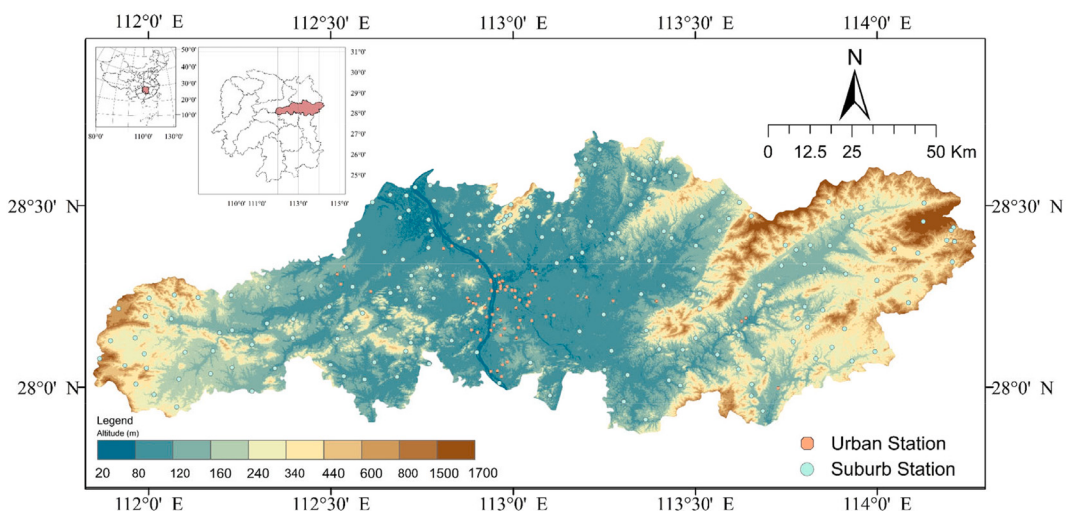


**Fig. 1.** The location of Changsha city and the meteorological stations.

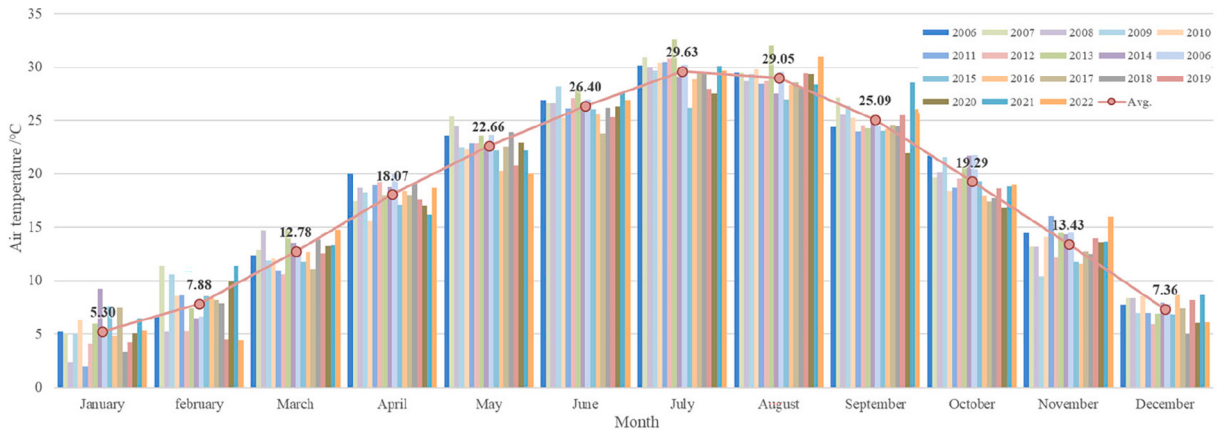


Fig. 2. Annual averages for Changsha's surface air temperature.

Collection of SAT data. Data sourced from the field measurements of the Changsha Meteorological Bureau <http://hn.cma.gov.cn/dsqx/zss/> and the research team, collecting the annual hourly temperature of the stations from 2018 to 2022, totaling approximately 10.95 million pieces of data. According to the longitude and latitude coordinates of the selected meteorological stations, ArcGIS was used to visualize the stations, and the stations were divided into urban stations (76) and suburb stations (204). The division of urban and suburb is based on Liu et al. (2023) findings, referring to the dataset of built-up areas of Chinese cities in 2020 (Sun et al., 2021). Since Landsat 8–9 acquired data in Changsha at 11:00 am (GMT Time 3:00), the SAT at the same time was selected for correlation analysis.

### 2.2.2. Land surface temperature

The study obtained Landsat 8–9 remote sensing data from the USGS Earth Explorer website (<https://earthexplorer.usgs.gov/>) to calculate LST. Since the revisit cycle of the Landsat satellite is 16 days, the influence of land cloud cover will affect the accuracy of the retrieval data (Gallo et al., 2011), resulting in data unavailable for several months. Therefore, many researchers only choose representative remote sensing images (Naim and Kafy, 2021; Rizvi et al., 2020; Tepanosyan et al., 2021) or use MODIS remote sensing data for research (Colaninno and Morello, 2022; Qin et al., 2022). Although MODIS remote sensing has a high temporal resolution (4 times a day), its low spatial resolution is 1000 m, which is unsuitable for studying fine-grained heterogeneous urban space, and there are significant errors in inverting the LST within the city. In contrast, the spatial resolution of Landsat 8–9 remote sensing data is 30 m, which has a higher spatial resolution than MODIS.

Consistent with the time of the SAT, select the Landsat 8–9 OLI/TIRS Collection 2 level 1 remote sensing image map from 2018 to 2022, and filter out the dates when the cloud cover is <10% in summer and winter. The remote sensing image of July 2018 strip number 123/40 with a cloud cover of 12.2% was still selected because Changsha crossed two zones. Another image with a stripe number of 123/41 had a cloud cover of 2.80%. Compared to the drawings, it was found that there were no clouds obstructing the study area, so this remote sensing image was selected. All the remote sensing images of 2021 have cloud cover >10%, so the data of this year is excluded. Table 1 summarizes the parameter information of the data.

Table 1  
The dates and related parameters of Landsat 8–9 remote sensing images.

Year	Season	Acquired data(m/d)	WRS Path/Row	Sun-Elevation	Sun-Azimuth	Land Cloud Cover	Avg. SAT (°C)
2018	Summer	7/29	123/40	65.77687608	109.24227220	12.2	3.0
		7/29	123/41	65.98676204	105.89471132	2.80	
	Winter	2/3	123/40	38.16358194	147.91984331	2.24	34.00
		2/3	123/41	39.24966683	147.01653769	1.32	
2019	Summer	8/17	123/40	63.45191278	120.35874986	2.13	33.0
		8/17	123/41	63.94150462	117.45567647	1.08	
	Winter	12/7	123/40	35.05669025	157.22491416	0.14	10.0
		12/7	123/41	36.28710652	156.53902428	0.08	
2020	Summer	8/3	123/40	65.27432146	112.38536985	5.61	31.0
		8/3	123/41	65.56427737	109.13729274	8.04	
	Winter	12/25	123/40	33.50019512	155.29162805	0.22	10.5
		12/25	123/41	34.70360411	154.60980959	0.44	
2022	Summer	8/9	123/40	64.62838227	115.68442646	0.89	33.0
		8/9	123/41	65.00174276	112.56316523	0.86	
	Winter	12/23	123/40	33.57809334	155.65608505	0.17	9.0
		12/23	123/41	34.78652738	154.97792735	2.25	

### 2.3. Methods

#### 2.3.1. LST inversion

There are mainly three types of surface temperature retrieval algorithms, the Radiative Transfer Equation, the Mono-Window Algorithm, and the Split-Window Algorithm. Scholars such as Yu et al. (2014) and Tang et al. (2017) have used these algorithms for surface temperature inversion, and this paper chooses the Mono-Window algorithm, which is an algorithm derived by Qin et al. (2001) based on the surface heat radiation conduction equation. Compared with the other two methods, the research shows that this algorithm can truly reflect LST and has high applicability. Landsat 8–9 OLI/TIRS remote sensing images are used in the radiative transfer, mainly including the following processes: radiation calibration, atmospheric correction, image mosaic, NDVI calculation, vegetation coverage calculation, TIRS band 10 brightness temperature calculation, land surface emissivity calculation, blackbody radiance calculation (at the same temperature), and LST calculation. The formula for the Mono-Window Algorithm is as follows:

$$T_s = [a(1 - C - D) + (b(2 - C - D) + C + D)T_{sensor} - DT_a]/C \quad (1)$$

Where  $T_s$  is the LST retrieved from the Landsat 8 TIRS Band 10 data;  $T_a$  is the effective mean atmospheric temperature;  $T_{sensor}$  is the brightness temperature of Landsat 8–9 TIRS Band 10;  $a$  and  $b$  are the coefficients used to approximate the derivative of the Planck radiance function for the TIRS Band 10,  $a = -67.355351$ ,  $b = 0.458606$ ; and  $C$  and  $D$  are the internal parameters for the algorithm based on the atmospheric parameters and ground emissivity.

#### 2.3.2. Urban heat island intensity calculation

The calculation of urban heat island intensity has been expressed differently in different studies, using the maximum air temperature in the city center minus the minimum value in the suburb (Anjos et al., 2020; Shirani-Bidabadi et al., 2019) or using the temperature in the urban area minus the average temperature in the suburb (El Kenawy et al., 2020; Zheng et al., 2022). To reduce the impact of variables, this study compared the differences between UHI and SUHI while ensuring consistency in the coordinates of SAT and LST. Changsha was divided into six districts based on its administrative regions, and suburb meteorological stations averages were calculated for each district, forming the basis for calculating the Urban Heat Island Index in each area. The calculation formula is as follows:

$$UHII = SAT_{urban} - SAT_{suburb} \quad (2)$$

$$SUHII = LST_{urban} - LST_{suburb} \quad (3)$$

#### 2.3.3. Correlation analysis

Statistical analysis was used to study the relationship between SAT and LST, analyzing the relationship between three years of simultaneous hourly data in winter and summer. Firstly, descriptive statistical analysis was performed on the two data groups to describe or summarize the characteristics of the data quantitatively. Secondly, a paired sample *t*-test was carried out to test whether there was a significant difference between the two data groups and to determine that the difference in the sample mean was not caused by sampling error. Further use Pearson correlation analysis and ordinary least squares (OLS) linear regression analysis to study the relationship between SAT and LST in summer and winter, and use Coefficient of Variation (C-V), *t*-test, and Effect size to prove. Among them, C-V can eliminate the influence of measurement scale and dimension and then compare the degree of dispersion of two sets of data (Sun et al., 2020). The smaller the C-V value, the smaller the deviation of the data. The calculation formula is as follows:

$$C.V = \frac{\sigma}{\mu} \times 100\% \quad (4)$$

$\sigma$  is the standard deviation of the sample, and  $\mu$  is the mean.

Paired *t*-test, also known as a related-sample *t*-test, is used to test whether there is a significant difference between two data groups and to determine whether the difference in sample means is not due to sampling error Resulting (McNemar, 1955). The calculation formula is as follows:

$$t = \frac{\bar{d}}{\sqrt{\frac{\sum d^2 - (\sum d)^2}{n(n-1)}}} \quad (5)$$

$n$  is the number of paired samples,  $d$  is the difference between each data pair and  $\bar{d}$  is the sample mean of the difference.

The result of the general significance test focuses on whether the *p* value is  $<0.001$ , indicating the probability that the difference in sample data can be attributed to chance alone (Cheng and Li, 2019). However, since the sample size affects the paired *t*-test value, it is proposed to interpret the *t*-test value through the effect size (Zheng and Wen Zl, 2011) indicators (Cohen's *d* and Glass's  $\Delta$ ). Cohen's *d* can indicate the standard difference between two means, unaffected by the sample size, and can obtain the importance of the independent variable to the dependent variable in the regression analysis. The calculation formula is as follows:

$$d = \frac{\mu_1 - \mu_2}{\sigma} \quad (6)$$

$\mu_1$  and  $\mu_2$  represent the mean of the two columns of data,  $\sigma$  represents the standard deviation of the population, and the values to measure the size are  $d = 0.2$  (small),  $d = 0.5$  (medium), and  $d = 0.8$  (big).

Glass's  $\Delta$  is generally used to compare two data groups when the sample size is relatively large and the variance is uneven, and it can better represent the overall standard deviation (Glass et al., 1981; Rosenthal, 1991). The calculation formula is as follows:

$$\Delta = \frac{\mu_1 - \mu_2}{S_2} \quad (7)$$

$\mu_1$  and  $\mu_2$  represent the mean of the two columns of data, and  $S_2$  represents the standard deviation of one data set.

#### 2.3.4. Error analysis

A set of statistical measures were calculated to evaluate the models' adjustment. The evaluation was performed by cross-validation, where the Root Mean Squared Error (RMSE) and the Mean Absolute Error (MAE) were calculated to assess the magnitude of the error between predicted and observed values. RMSE is particularly sensitive to outliers and was used to measure quadratic error individually (Janssen and Heuberger, 1995). At the same time, MAE is the average error size in a set of predictions considering the direction of the data. The calculation formula is as follows:

$$RMSE = \sqrt{\frac{\sum_{i=1}^n (X_{measure,i} - X_{model,i})^2}{n}} \quad (8)$$

$$MAE = n^{-1} \sum_{i=1}^n |X_{measure,i} - X_{model,i}| \quad (9)$$

$X_{measure}$  represents the temperature value of the observation point,  $X_{model}$  represents the model predicted temperature, and  $n$  represents the number of observation points.

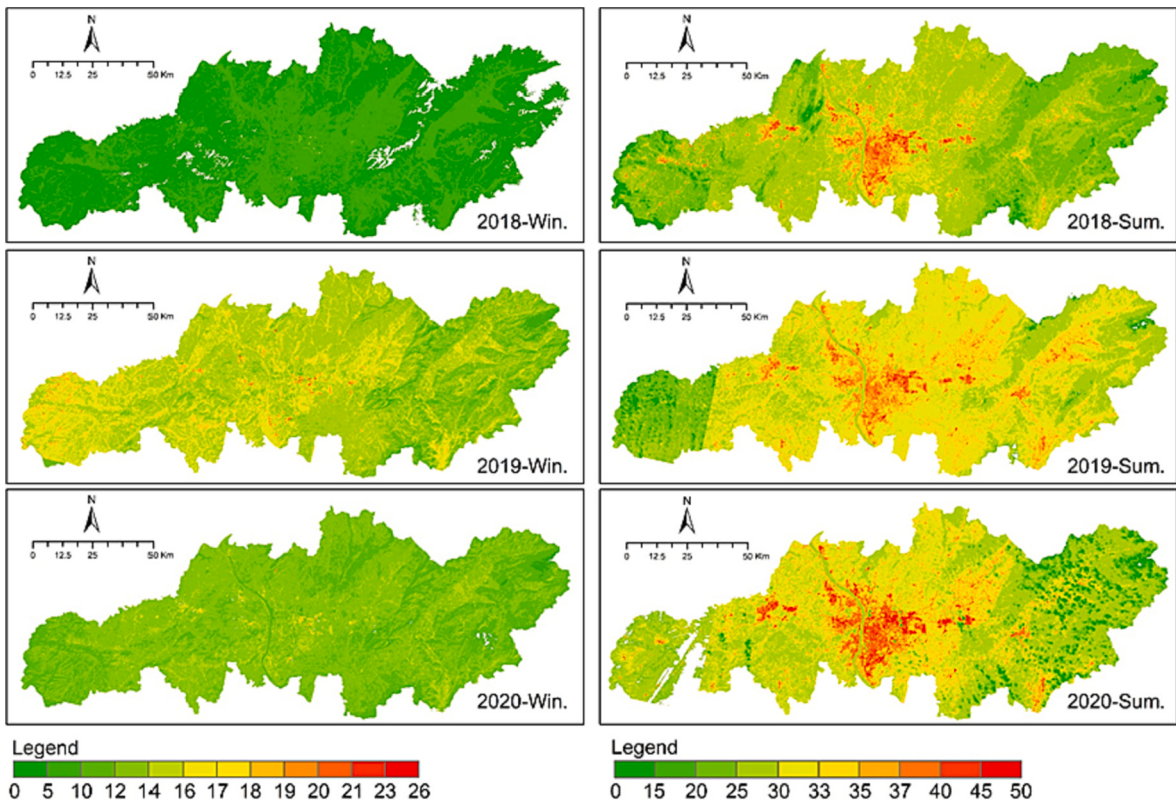


Fig. 3. Winter and summer LST inversions for 2018, 2019 and 2020.

### 3. Results

#### 3.1. Analysis of LST

Overview of LST data characteristics for different years. In 2018, winter data was concentrated between 4 and 8 °C, with a minimum temperature of -3 °C. At the end of July, the data concentrated between 19.8 and 38.4 °C, with a maximum temperature of 56.6 °C. In 2019, the LST in December were concentrated between 8.3 and 15.9 °C, with a minimum temperature of -1 °C. In August, during the summer, temperatures were concentrated between 24.2 and 37.6 °C, with a maximum temperature of 54.4 °C. In 2020, the LST in December were concentrated between 6.1 and 12.7 °C, with a minimum temperature of 0.5 °C. In August, during the summer, temperatures were concentrated between 19.7 and 39 °C, with the highest temperature reaching 61.2 °C.

Spatial differences in LST affected by season and underlying surface materials. As shown in Fig. 3, there are significant spatial variations and numerical differences in LST between winter and summer in Changsha. In winter, the differences in LST between urban and suburb areas are relatively small, with local hotspots reaching a maximum temperature of about 27 °C. In summer, the differences in LST between urban and suburb areas are much more pronounced, with urban temperatures much higher than those in suburb areas, with the highest temperature reaching about 61 °C. These results demonstrate that both time and underlying surface materials need to be considered when analyzing spatial variations in LST.

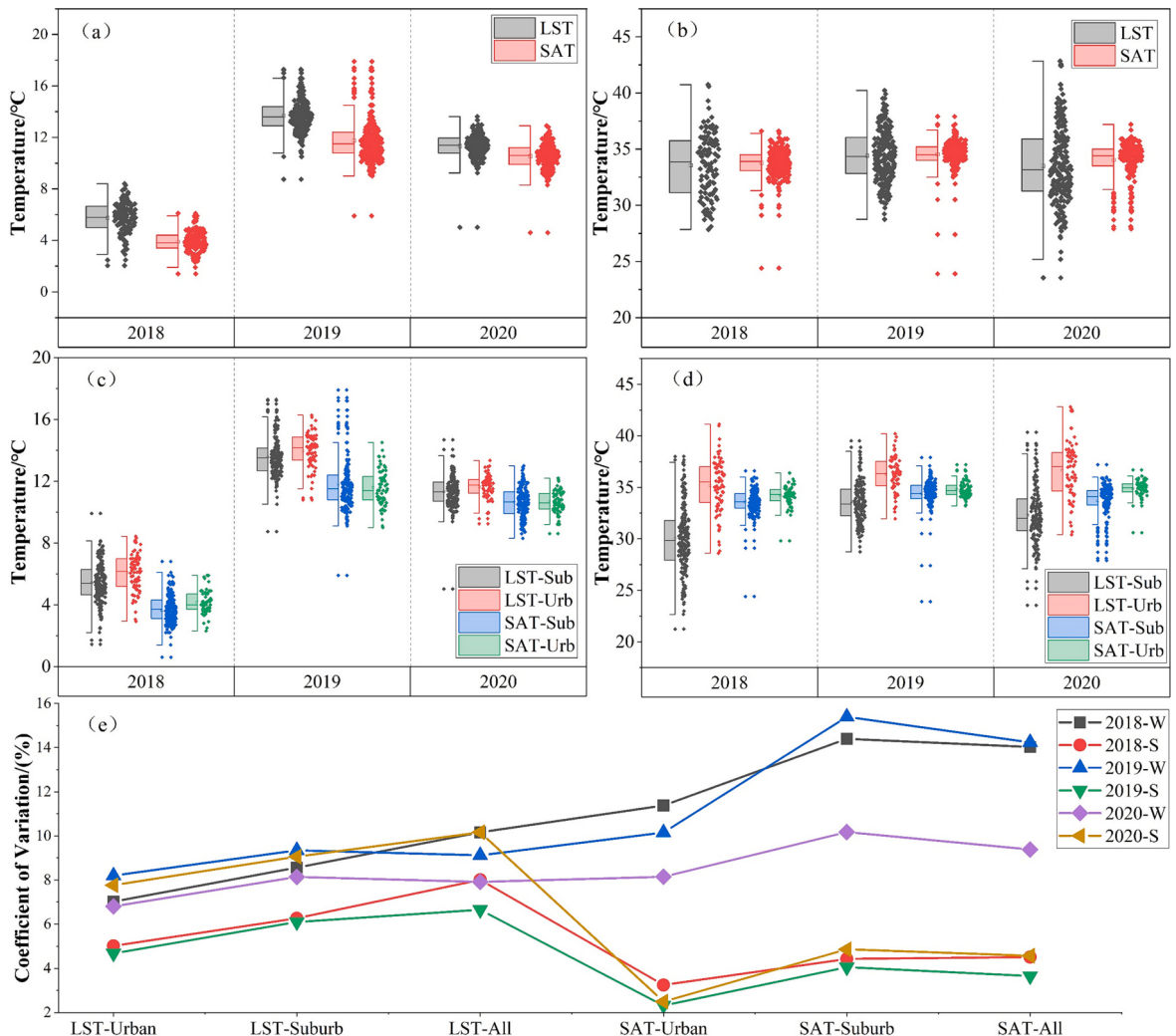


**Fig. 4.** Comparative analysis between LST and SAT: (a)-(b) temperature comparison in winter and summer; (c)-(d) comparison of urban and suburb in winter and summer, LST-urb, LST-sub, SAT-urb, and SAT-sub represent urban and suburb LST, urban and suburb SAT; (e) C·V for urban and suburb, denoted by W and S for winter and summer seasons, respectively.

### 3.2. Comparative analysis between LST and SAT

There are variations in SAT and LST across different seasons. Comparing data between winter and summer reveals that SAT is lower than LST in winter, with a relatively small numerical difference. In summer, SAT exceeds LST, and the range of LST values is significantly higher than that of SAT (Fig. 4a, b). In winter, the average difference is 1.83 °C, 1.92 °C, and 0.8 °C (representing the data of 2018, 2019, and 2020 respectively, the same below). In summer, the average difference is 0.22 °C, 0.14 °C, and 0.55 °C. Given that LST is affected by surface materials and spatial heterogeneity, the meteorological stations are categorized, and the differences between LST and SAT are compared between urban and suburb.

Significant differences exist in both SAT and LST between urban and suburb across different seasons. During winter, the disparities between urban and suburb are relatively small, with SAT and LST slightly higher in urban areas compared to suburb (Fig. 4c, d). The average temperature differences between  $LST_{urb}$  and  $LST_{sub}$  are 0.68 °C, 0.39 °C, and 0.40 °C, while the average temperature differences between  $SAT_{urb}$  and  $SAT_{sub}$  are 0.47 °C, 0.24 °C, and 0.14 °C. The average differences between  $LST_{urb}$  and  $SAT_{urb}$  are 1.74 °C, 1.95 °C, and 2.38 °C, with standard deviations are 0.34 °C, 1.66 °C, and 0.92 °C. The average differences between  $LST_{sub}$  and  $SAT_{sub}$  were 0.08 °C, 1.75 °C, and 0.72 °C, and the standard deviations were 1.53 °C, 1.80 °C, and 1.06 °C. In winter, there is a small difference between  $LST_{urb}$  and  $LST_{sub}$ ,  $SAT_{urb}$  and  $SAT_{sub}$ . Additionally, the difference between  $LST_{urb}$  and  $SAT_{urb}$ ,  $LST_{sub}$  and  $SAT_{sub}$  remain relatively consistent across different years. This finding demonstrates that the difference in LST and SAT between urban and suburb in winter is relatively minor and consistent over time.

The numerical differences are more pronounced in summer than in winter, especially between urban and suburb, where LST values significantly exhibiting exceed SAT.  $LST_{urb}$  exhibits notably higher value than  $LST_{sub}$ , with an average difference of 5.16 °C, 2.64 °C, and 4.37 °C, respectively. Similarly,  $SAT_{urb}$  demonstrates a slightly higher value than  $SAT_{sub}$ , with an average difference of 0.64 °C, 0.36 °C, and 1.20 °C. This contrast is particularly notable in winter. Additionally, the disparity between  $LST_{urb}$  and  $SAT_{urb}$  is relatively substantial, with an average difference of 1.01 °C, 1.47 °C, and 1.74 °C, accompanied by a standard deviation of 2.07 °C, 1.52 °C, and 2.28 °C. Unlike the winter,  $LST_{sub}$  shows lower values than  $SAT_{sub}$ , with an average difference of -3.56 °C, -0.81 °C, and -1.43 °C, and a standard deviation of 3.09 °C, 1.82 °C, and 2.40 °C. As a result, the overall average LST in the city is lower than that of SAT.

The C-V disparity are notably accentuated during winter and summer. During winter, both  $LST_{urb}$  and  $LST_{sub}$  exceed  $SAT_{urb}$  and  $SAT_{sub}$ , while in summer,  $LST_{urb}$  surpasses  $SAT_{urb}$ , and  $LST_{sub}$  falls below  $SAT_{sub}$ . These results explain the higher average SAT during summer in comparison to LST. Considering the variations in the number of meteorological stations and differences in surface materials between urban and suburb regions, further analysis will involve comparing and analyzing the C-V for additional verification. As per

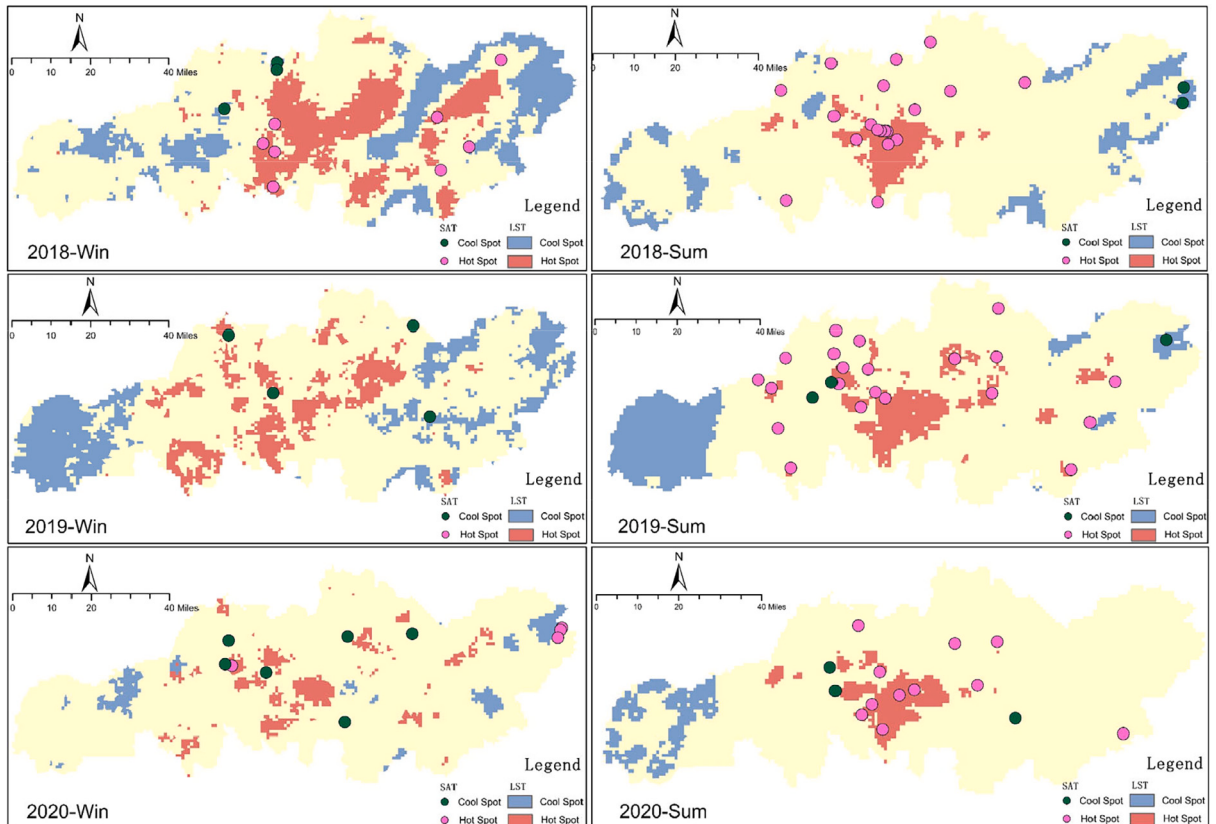
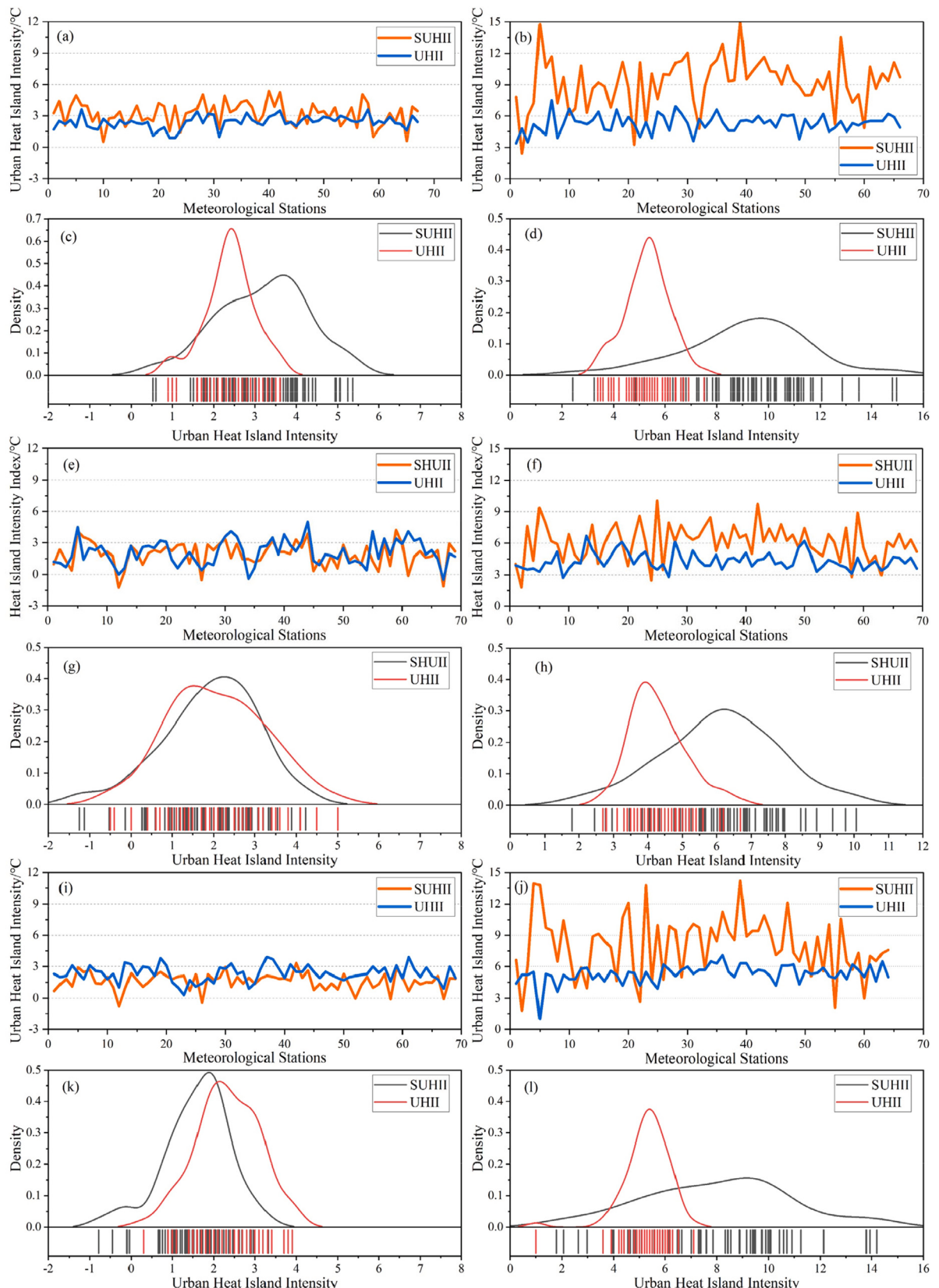


**Fig. 5.** The hotspots spatial distribution of SAT and LST.



(caption on next page)

**Fig. 6.** Statistical distributions and linear fittings between LST-UHII and SAT-UHII: (a) winter, (b) summer, (c) winter, and (d) summer in 2018; (e) winter and (f) summer, (g) winter, and (h) summer in 2019; and (i) winter, (j) summer, (k) winter, and (l) summer in 2020.

**Sun et al. (2020)**, LST exhibits greater temporal variability, which is supported by the findings illustrated in Fig. 4e. This figure illustrates heightened temporal variability in summer LST and winter SAT. During summer, the C-V value for SAT in urban remains relatively stable, at approximately 2.3%, whereas LST undergoes a change of approximately 6.1%.

### 3.3. Difference of heat island index between LST and SAT

Generally, the spatial pattern of LST different from that of SAT. Fig. 5 depicts the clustering analysis results of SAT and LST, indicating that the cold and hot spots of SAT-LST do not entirely overlap in space. During the summer, there is a greater overlap between the cold and hot spots of SAT and LST, with SAT's hot spots having a wider distribution than LST. LST's hot spots are concentrated within urban, whereas SAT's hotspots tend to appear in suburb. In winter, there is less overlap in spatial areas between cold and hot spots, and their spatial distribution is less concentrated compared to summer. According to the principles of the urban heat island effect, the clustering results of the heat island effect align with this, indicating that the cold and hot spots in the spatial distribution of UHI and SUHI do not overlap.

There are significant numerical differences between UHI and SUHI in winter and summer. Fig. 6 illustrates the variations in urban heat island intensity between SAT and LST across different seasons. This differs from the conclusion that SAT has a wider UHII range than LST in the study by **Sun et al. (2020)**, the urban heat island intensity of winter SAT is slightly greater than that of LST, while that of summer LST is much greater than that of SAT. In winter, SUHII is slightly higher than UHII, with a wider interval. Both SUHII and UHII are predominantly concentrated between 0 and 6 °C, averaging around 2.5 °C. Some meteorological stations, situated in vegetation or building shadow areas, result in negative SUHII values and lower than UHII. Conversely, in summer, SUHII significantly exceeds UHII. SUHII is clustered within the 4–12 °C range, with an average of approximately 9 °C. In contrast, UHII is centered around 4–6 °C, with an average around 5 °C, exhibiting a narrower numerical distribution. During winter, solar radiation has a minimal impact on LST, resulting in negligible changes in its values. Moreover, the trends in UHII and SUHII are largely consistent. However, in summer, UHII and SUHII display irregular patterns of variation, and they may even show opposite trends.

For example, consider the Qingzhuohu station located in the urban area, where the SUHII is measured at 13.81 °C and UHII at 1 °C. This station is situated near a school playground and adjacent to an arbor. However, it's important to note that the extraction of LST from Landsat8–9 satellite data, with its 30 m resolution, captures the center point of the affected pixel. As a result, the recorded LST value at the meteorological station can be influenced by the surrounding environment. In the case of the Qingzhuohu site, it happens to be surrounded by asphalt roads and outdoor sports venues, which further contribute to the local heat characteristics. This environmental influence leads to a notable difference between the LST at this station and the SAT obtained under the tree. Although SUHII has proven effective in evaluating urban heat island intensity, the disparities observed between SUHII and UHII during both winter and summer highlight the suitability of SAT for assessing urban heat island intensity over LST.

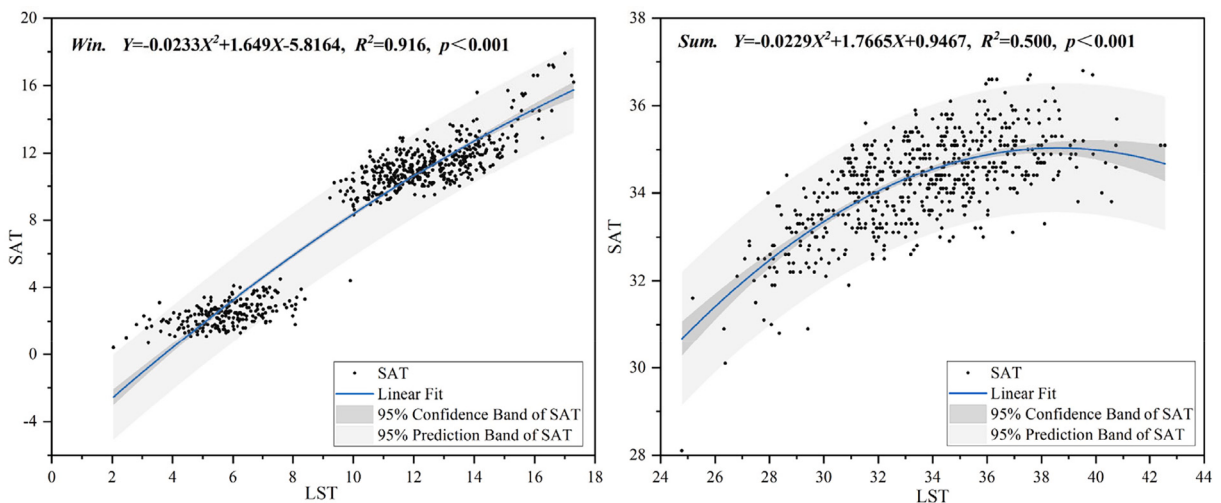


**Fig. 7.** The graphical representations of the two models.

### 3.4. Correlation analysis between LST and SAT

#### 3.4.1. Pearson analysis

In both summer and winter, LST had significantly positive correlations with SAT. The Pearson correlation coefficients between SAT and LST in winter were slightly greater than that in summer. Paired *t*-test for three years in winter and summer, and the average value of LST in winter is higher than that of SAT (*Mean* = 1.880 °C, *SD* = 1.470 °C, and *D-W test* = 1.237), *p* (Sig.) < 0.001, and the difference is statistically significant. The Pearson correlation result demonstrates a positive correlation of 0.955, followed by *t* = 33.171, Cohen's *d* = 0.477, Glass's  $\Delta$  = 0.542, 95% BCa CI [0.95; 0.96]. The data shows that the two have a small effect size, indicating that the two data groups have a very high correlation and smaller differences. The average value of LST in summer was lower than that of SAT (*Mean* = -0.682 °C, *SD* = 2.459 °C, and *D-W test* = 1.755), *p* (Sig.) < 0.001, and the difference was statistically significant. The Pearson correlation is 0.659, *t* = -6.709, Cohen's *d* = 0.301, Glass's  $\Delta$  = 0.645, 95% BCa CI [0.61; 0.70]. The effect size of the two data is medium, indicating that the two data groups have moderate correlation and smaller differences.

#### 3.4.2. Polynomial regression model

The winter's polynomial regression coefficient is higher than in summer, indicating a stronger relationship between LST and SAT (M.E., 2005), as illustrated in Fig. 7. The regression coefficient in winter is  $R^2 = 0.916$ , *p* (Sig.) < 0.001. LST will have a significant positive impact on SAT. The regression model exhibits a superior fit during winter, implying that LST explains 91.6% of the variability in SAT during this season. In summer, with a regression coefficient  $R^2 = 0.500$  and a significant *p*-value (*p* < 0.001), it indicates a moderate fit. There exists a linear relationship between the two variables, with LST explaining >50.02% of the variability in SAT. Significant differences in the correlation between LST and SAT during winter and summer necessitated the construction of two polynomial regression models to explain these variations. These models include a winter model (Formula 10) and a summer model (Formula 11).

$$Y = -0.0233X^2 + 1.649X - 5.8164 \quad (10)$$

$$Y = -0.0229X^2 + 1.7665X + 0.9467 \quad (11)$$

*X* represents the LST and *Y* represents the SAT.

### 3.5. Validation of the model

The accuracy of SAT predictions for both winter and summer falls within an acceptable margin of error. To verify this, we employed polynomial regression models acquired for temperature prediction during these seasons, utilizing data from August and December 2022. Initially, we obtained LST through the inversion of Landsat 8–9 remote sensing imagery. Subsequently, we processed the SAT data from meteorological stations, calculating the predicted SAT (P-SAT for short) based on the polynomial regression equation. Finally, we calculated the RMSE and MAE for both SAT and P-SAT. In Fig. 8, LST exhibits minimal variation, with an average value of approximately 12.3 °C, and the temperature difference between the urban and the suburb is about 0.24 °C. The SAT is slightly lower than the LST, with an average value of about 10.91 °C, and the temperature difference of approximately 0.17 °C between the urban and the suburb. The change of P-SAT closely mirrors that of SAT, with values close proximity. The average P-SAT value is about 11.27 °C, and the temperature difference between urban and suburb is roughly 0.27 °C. Regarding the RMSE of winter SAT versus P-SAT, ranged from 1.232 °C to 1.246 °C, and the MAE ranged from 1.008 °C to 1.010 °C. Generally, 1–2 °C is considered an accurate level of precision (Benali et al., 2012), and the values of the three spatial categories - urban, suburb, and city - meets these standards (Table 2).

During the summer, there are significant variations in LST between urban and suburb. Resulting in lower values for P-SAT. P-SAT data consistently fall below SAT, with suburb and city averages close to LST at around 35 °C, and the temperature difference between

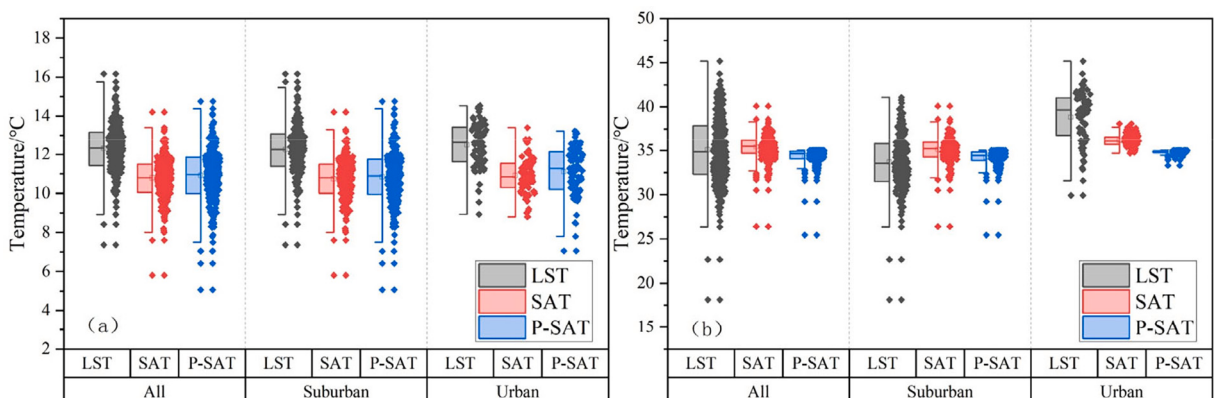


**Fig. 8.** Comparison and analysis of winter and summer data in 2022. (a): LST, SAT and P-SAT in winter and (b): LST, SAT and P-SAT in summer.

**Table 2**

The error analysis of polynomial regression model.

Season	RMSE-All (°C)	MAE-All (°C)	RMSE-Suburb (°C)	MAE- Suburb (°C)	RMSE-Urban (°C)	MAE- Urban (°C)
Winter	1.242	1.010	1.246	1.010	1.232	0.008
Summer	1.517	1.239	1.504	1.199	1.551	1.347

urban and suburb is approximately 0.6 °C. The RMSE of summer SAT versus P-SAT across the three spacial types ranges from 1.504 °C to 1.551 °C, and the MAE ranges from 1.199 °C to 1.347 °C, indicating overall high accuracy. This outcome underscores the reliability of the SAT prediction model based on polynomial regression.

#### 4. Discussion

##### 4.1. Spatial and season difference

LST and SAT originate from fundamentally vary mechanisms. The inherent discrepancy between LST and SAT result in varied numerical values, even when measured at the match time and geographic location. LST is the radiative skin temperature of ground. It depends on the albedo, the vegetation cover and the soil moisture, and responds rapidly to changes in incoming solar radiation due to cloud cover, aerosol load modifications, and diurnal variation of illumination. SAT quantifies the thermal content of the atmosphere, influenced by a multitude of factors, including incoming solar radiation, wind speed, humidity, and elevation. While both are affected by solar radiation, the key distinction lies in the fact that LST is influenced by surface material properties, whereas SAT is affected by various other meteorological elements within the air. Hence, the disparities between the two are unquestionably justified. Previous studies ([Liu et al., 2018](#); [Schwarz et al., 2012](#); [Sun et al., 2020](#); [Xiong and Chen, 2017](#)), have typically focused on individual time points or limited spatial types. However, this study selected Changsha, known for its hot summers and cold winters, as the research area, significantly expanding the dataset. Analyzed the differences between LST and SAT in winter and summer, urban and suburb, as well as the urban heat island effect. The research results provide a wealth of evidence supporting the substantial distinctions between these two temperature measurements.

The spatial disparities differences between winter and summer are notable. Undoubtedly, compared to summer, the decrease in the solar radiation angle in winter leads to lower values for both LST and SAT. In the winter, Changsha is influenced by the Siberian cold air mass, resulting in lower SAT values than the regional LST. In contrast, during the summer, under the influence of the same solar radiation, LST<sub>sub</sub> represents the temperature of the vegetation canopy, and its values is significantly lower compared to the SAT in the same area. SAT measurements are taken at pedestrian heights, which are affected by factors such as building shadows and vegetation cover, causing temperature variations over short distances ([Van Hove et al., 2015](#)). Additionally, remote sensing data acquisition is impacted by spatial accuracy and depends on the material at the pixel's center point. Consequently, it is crucial to account for the influence of seasons when utilizing SAT or LST.

The differences between urban and suburb, In winter, urban were generally exhibited higher temperatures than suburb for both LST and SAT (see [Fig. 4](#)). The distinct land cover types - urban and suburb - show significant differences in LST, whereas SAT have less variability. During summer, despite the considerable impact of intense solar radiation on LST, when considering the data from urban and suburb, SAT registers higher value than LST. This phenomenon can be attributed to the negative correlation between vegetation cover and LST, as supported by various studies ([Alavipanah et al., 2015](#); [Alvi et al., 2022](#); [Harun et al., 2020](#)). The LST of suburb is much lower than that in other regions, which also causes the urban-suburb difference in LST is much larger than in SAT. Nevertheless, according to [Fig. 4\(d\)](#), the variation in SAT between urban-suburb appears minimal in summer. This indicates that despite the presence of higher vegetation coverage in the suburb, the increase in SAT are only slight. Numerous studies focusing on LST ([Declet-Barreto et al., 2016](#); [Shiflett et al., 2017](#); [Xu et al., 2022](#)) have demonstrated that initiatives to enhance vegetation coverage in urban can mitigate urban warming. In contrast, the impact of vegetation on reducing SAT is less well understood, and the relationships between vegetation cover and SAT are more variable than those between vegetation and LST. Sampling campaigns aimed at assessing the effects of individual trees, green spaces, or the urban tree canopy have shown localized air cooling associated with vegetation ([Li et al., 2021](#); [Shi et al., 2020](#); [Zheng et al., 2018](#)). The findings of this study also further confirm that the effect of plants on LST and SAT differs, the cooling effects of vegetation within and among cities remain a persistent challenge. Variations in terrain elevation influence solar radiation, thereby indirectly impacting temperature fluctuations ([Good et al., 2017](#)). This effect is confirmed by [Fig. 4e](#), where urban exhibit a lower C·V value compared to suburb, further illustrating the influence of terrain ([Sun et al., 2020](#)).

##### 4.2. Discrepancy in the Urban Heat Island effect

The UHI and SUHI also exhibits disparities. During winter, the differences in SUHII and UHII values are relatively small, and their variations are quite consistent. However, in summer, the significant influence of solar radiation on surface temperatures leads to notably higher SUHII values compared to UHII. When comparing their C.V, significant differences are observed across different seasons. LST is more susceptible to surface materials and less stable, while SAT is less sensitive to urban spatial heterogeneity than LST. [Fig. 5](#) illustrates that the areas covered by SUHII and UHII do not entirely overlap. However, in most urban heat island studies, this phenomenon is often revealed by high-resolution LST data ([Guo et al., 2019](#)). In current UHI research, an increasing number of researchers ([Cheval and Dumitrescu, 2015](#); [Colaninno and Morello, 2022](#); [do Nascimento et al., 2022](#)) use SHUII instead of UHII to

evaluate the urban heat island intensity. Excessively high SHUII lead to significant differences in the research results and also cause urban residents' misperception of the urban thermal environment, resulting in psychological stress, environmental anxiety, or excessive energy use (Carter et al., 2016; Malone and Engle, 2011; Wan et al., 2022). Wang et al. (2019) also proved that the intensification of SHUII does not represent urban warming. Air temperature is the most direct indicator of residents' perception of the environment and is a crucial factor in evaluating urban thermal comfort. In terms of mitigating urban thermal effects, the strategy based on SAT proves to be more reliable. The results also underscore the importance of establishing a standardized meteorological network, facilitating finer-scale planning and design, as well as further exploration of urban spatiotemporal variations.

#### 4.3. The correlation between LST and SAT

The strongest Pearson correlations between the SAT and LST were higher in winter ( $r = 0.955, p < 0.000$ ) than in summer ( $r = 0.682, p < 0.000$ ). The data were verified by *t*-test, effect size Cohen's  $d$ , and Glass's  $\Delta$ , which proved that LST-SAT has a very high correlation and the difference is small. The model was verified using a new remote-sensing image and surface air temperature. The RMSE and MAE in winter are lower than those in summer, and the error in urban in winter is the smallest,  $RMSE = 1.232^{\circ}\text{C}$ ,  $MAE = 1.008^{\circ}\text{C}$ . In summer, the error in the suburb is also the smallest,  $RMSE = 1.504^{\circ}\text{C}$ ,  $MAE = 1.199^{\circ}\text{C}$ . Although the correlation coefficient in summer is lower than that of other studies (Cao et al., 2021; Sun et al., 2020), the values of RMSE and MAE (dos Santos, 2020; Yang et al., 2017) are minor. His results demonstrate seasonality's impact on model performance due to thermophysical different conditions between the seasons. The impact of seasonality on the model efficiency has also been found, e.g., by Alvi et al. (2022) and Rodriguez-Lado et al. (2007). Their study shows clearly lower fits in winter months, a phenomenon that was reversed with our study. Our research model demonstrates that the SAT-LST correlation is stronger in winter, and there is a greater variation in the SAT-LST relationship across cities with different latitudes and longitudes. However, the urban environment may modify the SAT-LST relationship but not depreciate the close connections.

Due to the limitations in data availability or data collection methods in the current urban heat island studies, many researchers (Li et al., 2021; Zheng et al., 2018) choose to focus on typical hot weather days or extreme weather days for their research. However, given the ongoing global climate change and the diverse spatial forms of urban, typical and extreme weather days are not representative, and relying solely on a limited number of SAT stations may not be suitable for developing spatial distribution models (Xiong and Chen, 2017). Therefore, to address the issue of limited meteorological data, Stewart and Oke (2012) proposed a classification standard for the local climate zone. The SAT-LST model constructed in this study can offer valuable data for investigating inter-zonal heat islands (Gál et al., 2015; Ng, 2015) and intra-zonal heat islands (Geletic et al., 2019; Kwok et al., 2019) within the local climate zone.

The SAT-LST model can forecast alterations in the thermal environment within urban planning schemes, thus helping to prevent local heat stress events in hot spots. LST can be calculated based on surface materials (Alvi et al., 2022; Goldblatt et al., 2021; Shiflett et al., 2017), enabling the effective identification of hotspots within urban areas and the corresponding changes in SAT. Furthermore, it is essential to implement effective strategies during the urban planning and design phases or establish high-temperature warning mechanisms (Cao et al., 2021; Horton et al., 2016) to mitigate excessive heat stress.

#### 4.4. Limitations and future research

This study constructed the SAT-LST model using temperature data from only four years, namely 2018, 2019, 2020, and 2022. Previous research has shown that the more sample data, the more accurate the simulation results will be. However, acquiring Landsat images with <10% cloud cover is particularly challenging given the local climate conditions in Changsha. An improvement in this regard is seen with Landsat 9 TIRS-2, which surpasses Landsat 8 TIRS in terms of acquiring remote sensing images. In future research, we intend to consider additional influencing factors to further enhance the model's accuracy. The study proposes SAT-LST correlations for both winter and summer. Subsequent work will delve deeper into the practical application of this model. It has the potential to be employed in various ways, such as incorporating urban spatial characteristics to develop strategies for mitigating urban heat. For instance, linking SAT with local climate zone classification, constructing the correlation between LST and thermal comfort, and then predicting the thermal comfort of spatial planning, this approach can contribute to the sustainable development of green and low-carbon cities.

### 5. Conclusion

In order to assess the urban heat island effect more effectively and explore the spatial and seasonal characteristics of SAT-LST, this study focuses on Changsha, a city known for its typical winter cold and summer heat patterns. We analyzed temperature data spanning the past four years to evaluate the consistency between SAT and LST. Furthermore, we have constructed seasonal polynomial regression equations to model the relationships between these variables. The results show that: (1) When a sufficient sample dataset is available, the seasonal changes in SAT and LST become more pronounced. SAT and LST exhibit varying correlations across different seasons, with  $R^2 = 0.916$  in winter and  $R^2 = 0.500$  in summer, both significance level of  $p = 0.001$ . Based on the data from 2022 for verification, the RMSE in winter is  $1.242^{\circ}\text{C}$ , while in summer, it is  $1.517^{\circ}\text{C}$ . The accuracy fall within the error range. (2) The seasonal characteristics of UHI and SUHI are different. During winter, there is an insignificant difference between them, but in summer, the rate of increase in LST surpasses that of SAT, leading to an increased difference between SUHI and UHI. These findings indicate that the reliability of either UHI or SUHI in characterizing long-term urban heat effects is limited. It is recommended to combine SAT and LST for a better capture of UHI features. (3) The research findings can be utilized to expand the dataset of SAT, predict or assess the UHI in

urban, and contribute to urban thermal environment research. To provide strategic support for addressing urban heat stress, data support for establishing standardized urban meteorological networks, and theoretical foundations for urban microclimate research. The research fills in the lack of fixed meteorological station data gaps in urban thermal environment research, provides a model for estimating pedestrian height SAT, and provides the possibility for related research on urban spatial development and UHI (non-SUHI).

## Funding

This work was supported by Hunan Provincial Natural Science Foundation General Project [No. 2023JJ30693], Hunan Provincial Social Science Achievement Evaluation Committee Key Project [No. XSP20ZDI021], Hunan Provincial Philosophy and Social Science Planning Fund Office [No. CX20220123] and Central South University Postgraduate Independent Exploration and Innovation Project [No. 2022ZZTS0031].

## CRediT authorship contribution statement

**Yanfen Xiang:** Conceptualization, Methodology, Visualization, Writing – original draft, Funding acquisition. **Bohong Zheng:** Supervision, Writing – review & editing, Funding acquisition. **Komi Bernard Bedra:** Investigation, Data curation, Writing – review & editing. **Qianli Ouyang:** Investigation, Formal analysis. **Junyou Liu:** Investigation, Formal analysis. **Jian Zheng:** Investigation, Methodology, Visualization, Writing – review & editing.

## Declaration of Competing Interest

The authors declare that they have no known competing financial interests or personal relationships that could have appeared to influence the work reported in this paper.

## Data availability

Data will be made available on request.

## References

- Alavipanah, S., Wegmann, M., Qureshi, S., Weng, Q., Koellner, T., 2015. The role of vegetation in mitigating urban land surface temperatures: a case study of Munich, Germany during the Warm Season. *Sustainability* 7, 4689–4706. <https://doi.org/10.3390/su7044689>.
- Alvi, U., Suomi, J., Kayhko, J., 2022. A cost-effective method for producing spatially continuous high-resolution air temperature information in urban environments. *Urban Clim.* 42. <https://doi.org/10.1016/j.uclim.2022.101123>.
- Anjos, M., Targino, A.C., Krecl, P., Okawa, G.Y., Braga, R.F., 2020. Analysis of the urban heat island under different synoptic patterns using local climate zones. *Build. Environ.* 185. <https://doi.org/10.1016/j.buildenv.2020.107268>.
- Basu, R., Ostro, B.D., 2008. A multicounty analysis identifying the populations vulnerable to mortality associated with high ambient temperature in California. *Am. J. Epidemiol.* 168, 632–637. <https://doi.org/10.1093/aje/kwn170>.
- Benali, A., Carvalho, A.C., Nunes, J.P., Carvalhais, N., Santos, A., 2012. Estimating air surface temperature in Portugal using MODIS LST data. *Remote Sens. Environ.* 124, 108–121. <https://doi.org/10.1016/j.rse.2012.04.024>.
- Cao, J., Zhou, W., Zheng, Z., Ren, T., Wang, W., 2021. Within-city spatial and temporal heterogeneity of air temperature and its relationship with land surface temperature. *Landsc. Urban Plan.* 206. <https://doi.org/10.1016/j.landurbplan.2020.103979>.
- Carter, T.R., Fronzek, S., Inkinen, A., Lahtinen, I., Lahtinen, M., Mela, H., et al., 2016. Characterising vulnerability of the elderly to climate change in the Nordic region. *Reg. Environ. Chang.* 16, 43–58. <https://doi.org/10.1007/s10113-014-0688-7>.
- Chen, G.Z., Hua, J.Y., Shi, Y., Ren, C., 2023a. Constructing air temperature and relative humidity-based hourly thermal comfort dataset for a high-density city using machine learning. *Urban Clim.* 47. <https://doi.org/10.1016/j.uclim.2022.101400>.
- Chen, Y.P., Li, J.Y., Hu, Y.Z., Liu, L.Y., 2023b. Spatial and temporal characteristics of nighttime UHII based on local climate zone scheme using mobile measurement-A case study of Changsha. *Build. Environ.* 228. <https://doi.org/10.1016/j.buildenv.2022.109869>.
- Cheng, K.M., Li, S.E., 2019. P-value in Scientific Research: Misunderstanding, P-hacking and Improvement Strategy. *J. Quantitative Tech. Econ.* 36, 117–136. <https://doi.org/10.13653/j.cnki.jqte.2019.07.007>.
- Cheval, S., Dumitrescu, A., 2015. The summer surface urban heat island of Bucharest (Romania) retrieved from MODIS images. *Theor. Appl. Climatol.* 121, 631–640. <https://doi.org/10.1007/s00704-014-1250-8>.
- Colaninno, N., Morello, E., 2022. Towards an operational model for estimating day and night instantaneous near-surface air temperature for urban heat island studies: outline and assessment. *Urban Clim.* 46. <https://doi.org/10.1016/j.uclim.2022.101320>.
- Coseo, P., Larsen, L., 2014. How factors of land use/land cover, building configuration, and adjacent heat sources and sinks explain Urban Heat Islands in Chicago. *Landsc. Urban Plan.* 125, 117–129. <https://doi.org/10.1016/j.landurbplan.2014.02.019>.
- Daly, C., Taylor, G., Gibson, W., 1997. The PRISM approach to mapping precipitation and temperature. In: Proc., 10th AMS Conf. on Applied Climatology, pp. 20–23 doi: 10.1.1.730.5725.
- Declet-Barreto, J., Knowlton, K., Jenerette, G.D., Buyantuev, A., 2016. Effects of urban vegetation on mitigating exposure of vulnerable populations to excessive heat in Cleveland, Ohio. *Weather Clim. Soc.* 8, 507–524. <https://doi.org/10.1175/Wcas-D-15-0026.1>.
- Di Piazza, A., Conti, F.L., Viola, F., Eccel, E., Noto, L.V., 2015. Comparative analysis of spatial interpolation methods in the Mediterranean area: application to temperature in Sicily. *Water* 7, 1866–1888. <https://doi.org/10.3390/w7051866>.
- do Nascimento, A.C.L., Galvani, E., Gobo, J.P.A., Wollmann, C.A., 2022. Comparison between air temperature and land surface temperature for the City of São Paulo, Brazil. *Atmosphere* 13. <https://doi.org/10.3390/atmos13030491>.
- dos Santos, R.S., 2020. Estimating spatio-temporal air temperature in London (UK) using machine learning and earth observation satellite data. *Int. J. Appl. Earth Obs. Geoinf.* 88. <https://doi.org/10.1016/j.jag.2020.102066>.
- El Kenawy, A.M., Hereher, M., Robaa, S.M., McCabe, M.E., Lopez-Moreno, J.I., Dominguez-Castro, F., et al., 2020. Nocturnal surface urban heat island over greater Cairo: spatial morphology, temporal trends and links to land-atmosphere influences. *Remote Sens.* 12. <https://doi.org/10.3390/rs12233889>.
- Eldrandaly, K.A., Abu-Zaid, M.S., 2011. Comparison of six GIS-based spatial interpolation methods for estimating air temperature in Western Saudi Arabia. *J. Environ. Inf.* 18, 38–45. <https://doi.org/10.3808/jei.201100197>.

- Gál, T., Bechtel, B., Unger, J., 2015. Comparison of two different local climate zone mapping methods. In: ICUC9: The 9th International Conference on Urban Climate, France: Toulouse. [http://real.mtak.hu/28577/1/GD2-6-1551002\\_a.pdf](http://real.mtak.hu/28577/1/GD2-6-1551002_a.pdf).
- Gallo, K., Hale, R., Tarpley, D., Yu, Y.Y., 2011. Evaluation of the relationship between air and land surface temperature under clear- and cloudy-sky conditions. *J. Appl. Meteorol. Climatol.* 50, 767–775. <https://doi.org/10.1175/2010jamc2460.1>.
- Geletic, J., Lehnert, M., Savic, S., Milosevic, D., 2019. Inter-/intra-zonal seasonal variability of the surface urban heat island based on local climate zones in three central European cities. *Build. Environ.* 156, 21–32. <https://doi.org/10.1016/j.buildenv.2019.04.011>.
- Glass, G.V., McGaw, B., Smith, M.L., 1981. Meta-Analysis in Social Research. SAGE Publications, Inc., Beverly Hills [https://doi.org/10.1016/0149-7189\(82\)90011-8](https://doi.org/10.1016/0149-7189(82)90011-8).
- Goldblatt, R., Addas, A., Crull, D., Maghrabi, A., Levin, G.G., Rubinyi, S., 2021. Remotely sensed derived land surface temperature (LST) as a proxy for air temperature and thermal comfort at a small geographical scale. *Land* 10. <https://doi.org/10.3390/land10040410>.
- Good, E., 2015. Daily minimum and maximum surface air temperatures from geostationary satellite data. *J. Geophys. Res.-Atmos.* 120, 2306–2324. <https://doi.org/10.1002/2014jd022438>.
- Good, E.J., Ghent, D.J., Bulgin, C.E., Remedios, J.J., 2017. A spatiotemporal analysis of the relationship between near-surface air temperature and satellite land surface temperatures using 17 years of data from the ATSR series. *J. Geophys. Res.-Atmos.* 122, 9185–9210. <https://doi.org/10.1002/2017jd026880>.
- Guo, X., Huang, G., Jia, P., Wu, J.G., 2019. Estimating fine-scale heat vulnerability in Beijing through two approaches: spatial patterns, similarities, and divergence. *Remote Sens.* 11 (20) <https://doi.org/10.3390/rs11202358>.
- Harun, Z., Reda, E., Abdulrazzaq, A., Abbas, A.A., Yusup, Y., Zaki, S.A., 2020. Urban heat island in the modern tropical Kuala Lumpur: comparative weight of the different parameters. *Alex. Eng. J.* 59, 4475–4489. <https://doi.org/10.1016/j.aej.2020.07.053>.
- He, B.J., Wang, J.S., Liu, H.M., Ulpiani, G., 2021. Localized synergies between heat waves and urban heat islands: implications on human thermal comfort and urban heat management. *Environ. Res.* 193. <https://doi.org/10.1016/j.envres.2020.110584>.
- He, B.J., Wang, J.S., Zhu, J., Qi, J.D., 2022. Beating the urban heat: Situation, background, impacts and the way forward in China. *Renew. Sustain. Energy Rev.* 161. <https://doi.org/10.1016/j.rser.2022.112350>.
- Horton, R.M., Mankin, J.S., Lesk, C., Coffel, E., Raymond, C., 2016. A review of recent advances in research on extreme heat events. *Curr. Clim. Change Rep.* 2, 242–259. <https://doi.org/10.1007/s40641-016-0042-x>.
- Howard, L., 1833. *The Climate of London Deduced from Meteorological Observations Made in the Metropolis and at Various Places around it*. London Harvey and Darton, London.
- Hu, L.Q., Brunsell, N.A., 2015. A new perspective to assess the urban heat island through remotely sensed atmospheric profiles. *Remote Sens. Environ.* 158, 393–406. <https://doi.org/10.1016/j.rse.2014.10.022>.
- Huang, X.Z., Yao, R.M., Xu, T.T., Zhang, S.X., 2023. The impact of heatwaves on human perceived thermal comfort and thermal resilience potential in urban public open spaces. *Build. Environ.* 242. <https://doi.org/10.1016/j.buildenv.2023.110586>.
- Intergovernmental Panel on Climate (IPCC), 2021. Climate Change 2021: The Physical Science Basis - Summary for Policymakers (AR6). IPCC, Switzerland. [http://refhub.elsevier.com/S0048-9697\(22\)06891-7/rf202210300908168874](http://refhub.elsevier.com/S0048-9697(22)06891-7/rf202210300908168874).
- Ivajncic, D., Kaligacic, M., Ziberna, I., 2014. Geographically weighted regression of the urban heat island of a small city. *Appl. Geogr.* 53, 341–353. <https://doi.org/10.1016/j.apgeog.2014.07.001>.
- Janssen, P.H.M., Heuberger, P.S.C., 1995. Calibration of process-oriented models. *Ecol. Model.* 83, 55–66. [https://doi.org/10.1016/0304-3800\(95\)00084-9](https://doi.org/10.1016/0304-3800(95)00084-9).
- Jeffrey, S.J., Carter, J.O., Moodie, K.B., Beswick, A.R., 2001. Using spatial interpolation to construct a comprehensive archive of Australian climate data. *Environ. Model. Softw.* 16, 309–330. [https://doi.org/10.1016/S1364-8152\(01\)00008-1](https://doi.org/10.1016/S1364-8152(01)00008-1).
- Kousis, I., Pigliatiello, I., Pisello, A.L., 2023. Investigating the intra-urban thermal and air quality environment: new transect sensing methodology and measurements. *Measurement* 219. <https://doi.org/10.1016/j.measurement.2023.113210>.
- Kwok, Y.T., Schoetter, R., Lau, K.K.L., Hidalgo, J., Ren, C., Pigeon, G., et al., 2019. How well does the local climate zone scheme discern the thermal environment of Toulouse (France)? An analysis using numerical simulation data. *Int. J. Climatol.* 39, 5292–5315. <https://doi.org/10.1002/joc.6140>.
- Li, J.Y., Zheng, B.H., Ouyang, X., Chen, X., Bedra, K.B., 2021. Does shrub benefit the thermal comfort at pedestrian height in Singapore? *Sustain. Cities Soc.* 75. <https://doi.org/10.1016/j.scs.2021.103333>.
- Liu, D.W., Grimmond, C.S.B., Tan, J.G., Ao, X.Y., Peng, J., Cui, L.L., et al., 2018. A new model to downscale urban and rural surface and air temperatures evaluated in Shanghai, China. *J. Appl. Meteorol. Climatol.* 57, 2267–2283. <https://doi.org/10.1175/Jamc-D-17-0255.1>.
- Liu, Z., Cai, W., Luo, Y., Gong, P., 2021. Understanding the 2020 lancet countdown: human health and climate change report. *Sci. Technol. Rev.* 39, 24–31. <https://doi.org/10.3981/j.issn.1000-7857.2021.19.003>.
- Liu, Y., Ortega-Farias, S., Tian, F., Wang, S.F., Li, S., 2021a. Estimation of surface and near-surface air temperatures in arid Northwest China using landsat satellite images. *Front. Environ. Sci.* 9. <https://doi.org/10.3389/fenvs.2021.791336>.
- Liu, H.M., He, B.J., Gao, S.H., Zhan, Q.M., Yang, C., 2023. Influence of non-urban reference delineation on trend estimate of surface urban heat island intensity: a comparison of seven methods. *Remote Sens. Environ.* 296. <https://doi.org/10.1016/j.rse.2023.113735>.
- M.E., 2005. Chapter 56 - Karl Pearson, paper on the chi square goodness of fit test (1900). Author links open overlay panel M.E. Magnello. In: M. Landmark Writings in Western Mathematics 1640–1940. Elsevier B.V., pp. 724–731
- Malone, E.L., Engle, N.L., 2011. Evaluating regional vulnerability to climate change: purposes and methods. *Wiley Interdiscip. Rev. Clim. Chang.* 2, 462–474. <https://doi.org/10.1002/wcc.116>.
- Manley, G., 1958. On the frequency of snowfall in metropolitan England. *Q. J. R. Meteorol. Soc.* 84, 70–72. <https://doi.org/10.1002/qj.49708435910>.
- Manoli, G., Fatici, S., Schlapfer, M., Yu, K.L., Crowther, T.W., Meili, N., et al., 2019. Magnitude of urban heat islands largely explained by climate and population. *Nature* 573, 55. <https://doi.org/10.1038/s41586-019-1512-9>.
- McNemar, Q., 1955. Psychological Statistics, 2nd ed. John Wiley, Oxford, England. <https://doi.org/10.1126/science.122.3159.125a>.
- Memon, R.A., Leung, D.Y.C., Liu, C.H., 2009. An investigation of urban heat island intensity (UHII) as an indicator of urban heating. *Atmos. Res.* 94, 491–500. <https://doi.org/10.1016/j.atmosres.2009.07.006>.
- Mirzaei, P.A., 2015. Recent challenges in modeling of urban heat island. *Sustain. Cities Soc.* 19, 200–206. <https://doi.org/10.1016/j.scs.2015.04.001>.
- Naim, M.N.H., Kafy, A.-A., 2021. Assessment of urban thermal field variance index and defining the relationship between land cover and surface temperature in Chattogram city: a remote sensing and statistical approach. *Environ. Chall.* 4, 100107 <https://doi.org/10.1016/j.envc.2021.100107>.
- Ng, Y.X., 2015. A study of urban heat island using “Local Climate Zones” – the case of Singapore. *Br. J. Environ. Clim. Change* 5, 116–133. <https://doi.org/10.9734/BJECC/2015/13051>.
- Nichol, J.E., Wong, M.S., 2008. Spatial variability of air temperature and appropriate resolution for satellite-derived air temperature estimation. *Int. J. Remote Sens.* 29, 7213–7223. <https://doi.org/10.1080/01431160802192178>.
- Oke, T.R., 1982. The energetic basis of the urban heat island. *Q. J. R. Meteorol. Soc.* 108, 1–24. <https://doi.org/10.1002/qj.49710845502>.
- Oke, T.R., Johnson, G.T., Steyn, D.G., Watson, I.D., 1991. Simulation of surface urban heat islands under ‘ideal’ conditions at night part 2: diagnosis of causation. *Bound.-Layer Meteorol.* 56, 339–358. <https://doi.org/10.1007/BF00119211>.
- Qin, Z., Zhang, M., Karnieli, A., Berliner, P., 2001. Mono-window algorithm for retrieving land surface temperature from Landsat TM data. *Acta Geograph. Sin.* 56, 456–466. <https://doi.org/10.11821/xb200104009>.
- Qin, J., He, M., Jiang, H., Lu, N., 2022. Reconstruction of 60-year (1961–2020) surface air temperature on the Tibetan Plateau by fusing MODIS and ERA5 temperatures. *Sci. Total Environ.* 853. <https://doi.org/10.1016/j.scitotenv.2022.158406>.
- Reiners, P., Sobrino, J., Kuenzer, C., 2023. Satellite-derived land surface temperature dynamics in the context of global change – a review. *Remote Sens.* 15, 1857. <https://doi.org/10.3390/rs15071857>.
- Rizvi, S.H., Fatima, H., Iqbal, M.J., Alam, K., 2020. The effect of urbanization on the intensification of SUHIs: analysis by LULC on Karachi. *J. Atmos. Sol. Terr. Phys.* 207. <https://doi.org/10.1016/j.jastp.2020.105374>.

- Rodriguez-Lado, L., Sparovek, G., Vidal-Torrado, P., Dourado Neto, D., Macias-Vazquez, F., 2007. Modelling air temperature for the state of São Paulo, Brazil. *Sci. Agric.* 64, 460–467. <https://doi.org/10.1590/S0103-90162007000500002>.
- Rosenthal, R., 1991. Meta-Analytic Procedures for Social Research, , Rev. ed.vol. 6. SAGE Publications, Inc., Newbury Park <https://doi.org/10.4135/9781412984997>.
- Schwarz, N., Schlink, U., Franck, U., Großmann, K., 2012. Relationship of land surface and air temperatures and its implications for quantifying urban heat island indicators—an application for the city of Leipzig (Germany). *Ecol. Indic.* 18, 693–704. <https://doi.org/10.1016/j.ecolind.2012.01.001>.
- Sheng, L., Tang, X., You, H., Gu, Q., Hu, H., 2017. Comparison of the urban heat island intensity quantified by using air temperature and Landsat land surface temperature in Hangzhou, China. *Ecol. Indic.* 72, 738–746. <https://doi.org/10.1016/j.ecolind.2016.09.009>.
- Shi, L.H., Liu, P.F., Kloog, I., Lee, M., Kosheleva, A., Schwartz, J., 2016. Estimating daily air temperature across the southeastern United States using high-resolution satellite data: a statistical modeling study. *Environ. Res.* 146, 51–58. <https://doi.org/10.1016/j.envres.2015.12.006>.
- Shi, D.C., Song, J.Y., Huang, J.X., Zhuang, C.Q., Guo, R., Gao, Y.F., 2020. Synergistic cooling effects (SCEs) of urban green-blue spaces on local thermal environment: a case study in Chongqing, China. *Sustain. Cities Soc.* 55. <https://doi.org/10.1016/j.scs.2020.102065>.
- Shiflett, S.A., Liang, L.Y.L., Crum, S.M., Feyisa, G.L., Wang, J., Jenerette, G.D., 2017. Variation in the urban vegetation, surface temperature, air temperature nexus. *Sci. Total Environ.* 579, 495–505. <https://doi.org/10.1016/j.scitotenv.2016.11.069>.
- Shirani-Bidabadi, N., Nasrabadi, T., Faryadi, S., Larijani, A., Shadman Roodposhti, M., 2019. Evaluating the spatial distribution and the intensity of urban heat island using remote sensing, case study of Isfahan city in Iran. *Sustain. Cities Soc.* 45, 686–692. <https://doi.org/10.1016/j.scs.2018.12.005>.
- Stewart, I.D., Oke, T.R., 2012. Local climate zones for urban temperature studies. *Bull. Am. Meteorol. Soc.* 93, 1879–1900. <https://doi.org/10.1175/Bams-D-11-00019.1>.
- Stisen, S., Sandholt, I., Norgaard, A., Fensholt, R., Eklundh, L., 2007. Estimation of diurnal air temperature using MSG SEVIRI data in West Africa. *Remote Sens. Environ.* 110, 262–274. <https://doi.org/10.1016/j.rse.2007.02.025>.
- Sun, T., Sun, R., Chen, L., 2020. The trend inconsistency between land surface temperature and near surface air temperature in assessing urban heat island effects. *Remote Sens.* 12, 1271. <https://doi.org/10.3390/rs12081271>.
- Sun, Z., Sun, J., Guo, H., Jiang, H., Gao, J., Wang, J., 2021. A dataset of built-up areas of Chinese cities in 2020. In: Bank SD, editor. <https://doi.org/10.11922/scientedb.j00001.00332>.
- Tang, B.H., Zhan, C., Li, Z.L., Wu, H., Tang, R.L., 2017. Estimation of land surface temperature from MODIS data for the atmosphere with air temperature inversion profile. *IEEE J. Sel. Top. Appl. Earth Obs. Remote Sens.* 10, 2976–2983. <https://doi.org/10.1109/Jstars.2016.2634629>.
- Tepanosyan, G., Muradyan, V., Hovsepyan, A., Pinigin, G., Medvedev, A., Asmaryan, S., 2021. Studying spatial-temporal changes and relationship of land cover and surface Urban Heat Island derived through remote sensing in Yerevan, Armenia. *Build. Environ.* 187. <https://doi.org/10.1016/j.buildenv.2020.107390>.
- Van Hove, L.W.A., Jacobs, C.M.J., Heusinkveld, B.G., et al., 2015. Temporal and spatial variability of urban heat island and thermal comfort within the Rotterdam agglomeration. *Build. Environ.* (83), 91–103. <https://doi.org/10.1016/j.buildenv.2014.08.029>.
- Van Tol, Z., Ellis, A., 2023. Analysis of urban Heat Island intensity through air mass persistence: a case study of four United States cities. *Urban Clim.* 47. <https://doi.org/10.1016/j.uclim.2022.101345>.
- Vogt, J.V., Viau, A.A., Paquet, F., 1997. Mapping regional air temperature fields using satellite-derived surface skin temperatures. *Int. J. Climatol.* 17, 1559–1579. [https://doi.org/10.1002/\(SICI\)1097-0088\(19971130\)17:14<1559::AID-JOC211>3.0.CO;2-5](https://doi.org/10.1002/(SICI)1097-0088(19971130)17:14<1559::AID-JOC211>3.0.CO;2-5).
- Voogt, J.A., Oke, T.R., 2003. Thermal remote sensing of urban climates. *Remote Sens. Environ.* 86, 370–384. [https://doi.org/10.1016/S0034-4257\(03\)00079-8](https://doi.org/10.1016/S0034-4257(03)00079-8).
- Wan, K., Feng, Z.Q., Hajat, S., Doherdy, R.M., 2022. Temperature-related mortality and associated vulnerabilities: evidence from Scotland using extended time-series datasets. *Environ. Health* 21. <https://doi.org/10.1186/s12940-022-00912-5>.
- Wang, J., Zhou, W.Q., Wang, J., 2019. Time-series analysis reveals intensified urban heat island effects but without significant urban warming. *Remote Sens.* 11. <https://doi.org/10.3390/rs11192229>.
- Xiong, Y., Chen, F., 2017. Correlation analysis between temperatures from Landsat thermal infrared retrievals and synchronous weather observations in Shenzhen, China. *Remote Sens. Appl. Soc. Environ.* 7, 40–48. <https://doi.org/10.1016/j.rsase.2017.06.002>.
- Xu, C., Chen, G.D., Huang, Q.Y., Su, M.R., Rong, Q.Q., Yue, W.C., et al., 2022. Can improving the spatial equity of urban green space mitigate the effect of urban heat islands? An empirical study. *Sci. Total Environ.* 841. <https://doi.org/10.1016/j.scitotenv.2022.156687>.
- Xu, T.T., Yao, R.M., Du, C.Q., Li, B.Z., Fang, F.X., 2023. A quantitative evaluation model of outdoor dynamic thermal comfort and adaptation: a year-long longitudinal field study. *Build. Environ.* 237. <https://doi.org/10.1016/j.buildenv.2023.110308>.
- Yang, Y., Cai, W., Yang, J., 2017. Evaluation of MODIS land surface temperature data to estimate near-surface air temperature in Northeast China. *Remote Sens.* 9. <https://doi.org/10.3390/rs9050410>.
- Yang, Y.Z., Cai, W.H., Yang, J., 2017b. Evaluation of MODIS land surface temperature data to estimate near-surface air temperature in Northeast China. *Remote Sens.* 9. <https://doi.org/10.3390/rs9050410>.
- Yang, C., Wang, R., Zhang, S., Ji, C., Fu, X., 2019. Characterizing the hourly variation of urban heat islands in a snowy climate city during summer. *Int. J. Environ. Res. Public Health* 16, 2467. <https://doi.org/10.3390/ijerph16142467>.
- Yu, X., Guo, X., Wu, Z., 2014. Land surface temperature retrieval from Landsat 8 TIRS—comparison between radiative transfer equation-based method, split window algorithm and single channel method. *Remote Sens.* 6, 9829–9852. <https://doi.org/10.3390/rs6109829>.
- Zheng, H.M., Wen Zl, Wu Y., 2011. The appropriate effect sizes and their calculations in psychological research. *Adv. Psychol. Sci.* 19, 1868–1878. <https://journal.psych.ac.cn/adps/EN>.
- Zheng, B.H., Bedra, K.B., Zheng, J., Wang, G.G., 2018. Combination of tree configuration with street configuration for thermal comfort optimization under extreme summer conditions in the Urban Center of Shantou City, China. *Sustainability* 10. <https://doi.org/10.3390/su1014192>.
- Zheng, B.H., Chen, Y.P., Hu, Y.Z., 2022. Analysis of land cover and SUHII pattern using local climate zone framework – a case study of Chang-Zhu-Tan main urban area. *Urban Clim.* 43. <https://doi.org/10.1016/j.uclim.2022.101153>.